

Supporting information for

Spin Crossover Properties of Enantiomers, Co-enantiomers, Racemates, and Co-racemates.

Long-Fang Qin,^a Chun-Yan Pang,^a Wang-Kang Han,^a Feng-Li Zhang,^a Lei Tian,^a Zhi-Guo Gu,^{*a} Xuehong Ren,^b and Zaijun Li^a

^a The Key Laboratory of Food Colloids and Biotechnology Ministry of Education, School of Chemical and Material Engineering, Jiangnan University, Wuxi 214122, China.

^b The Key Laboratory of Eco-textiles of Ministry of Education, College of Textiles and Clothing, Jiangnan University, Wuxi 214122, China

| Table of contents | |
|-------------------------------------|---------|
| 1. Single crystal structures | S2 |
| 2. Intramolecular interactions | S3-S4 |
| 3. Intermolecular interactions | S5 |
| 4. UV/Vis and CD spectra | S6-S7 |
| 5. Thermogravimetric analyses (TGA) | S8-S9 |
| 6. Variable-temperature PXRD | S10-S13 |
| 7. Mössbauer data | S14-S17 |
| 8. Crystallographic data | S18-S25 |
| 9. Reference | S26 |

1. Single crystal structures

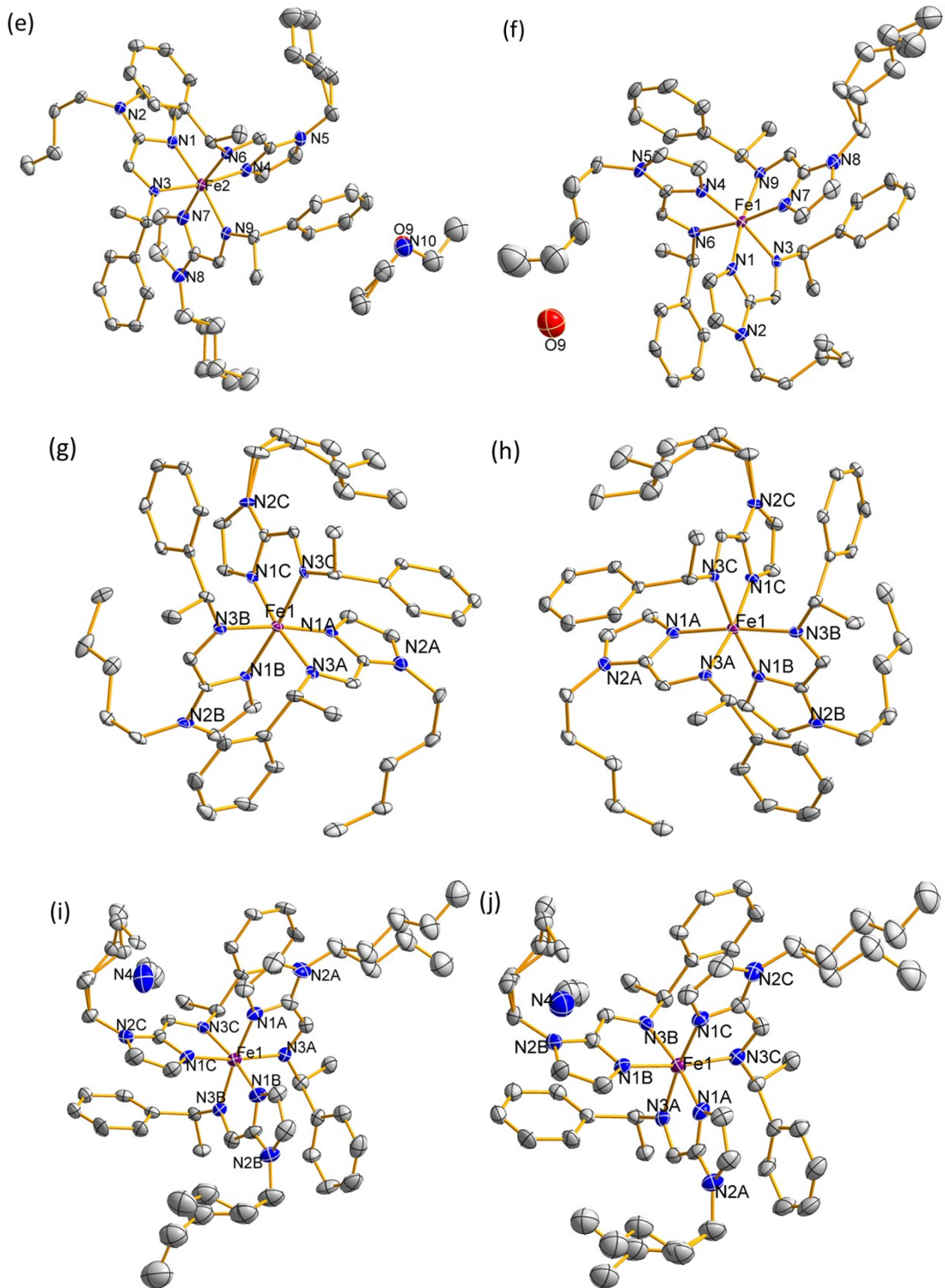
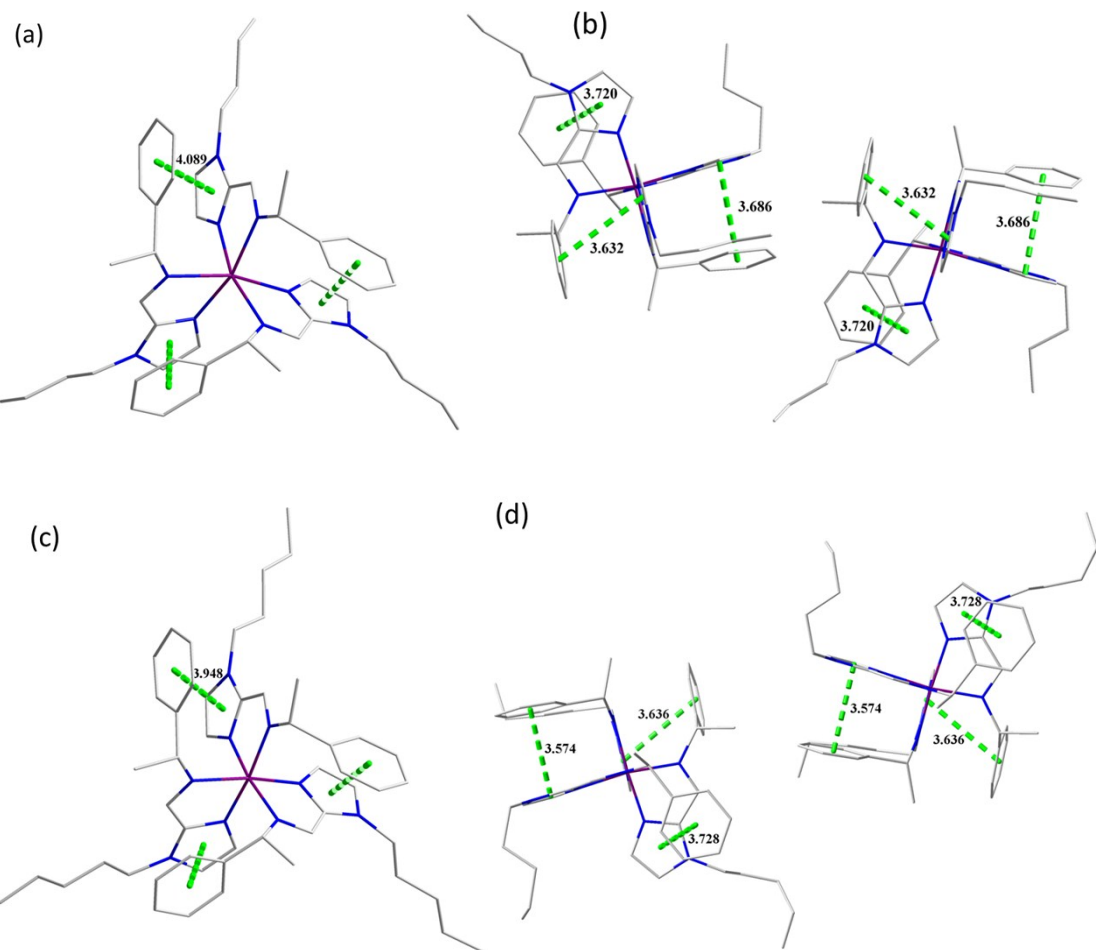
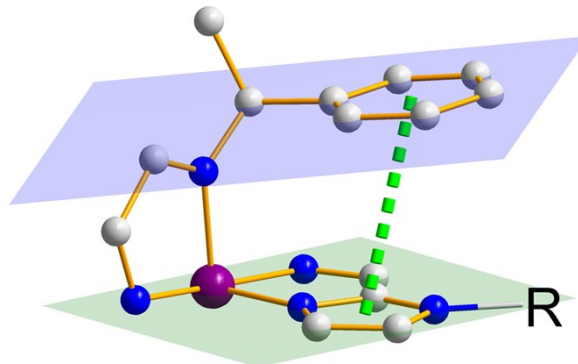


Fig. S1. Single crystal structures of **4RS** (e), **5RS** (f), **4R5R** (g), **4S5S** (h), **4S5R** (i) and **4R5S** (j). Color code: C, gray; N, blue; Fe, violet. H atoms and counterions are omitted for clarity, while the remaining atoms are represented by anisotropic displacement parameter ellipsoids at a 30% probability level.

2. Intramolecular π - π stacking interactions



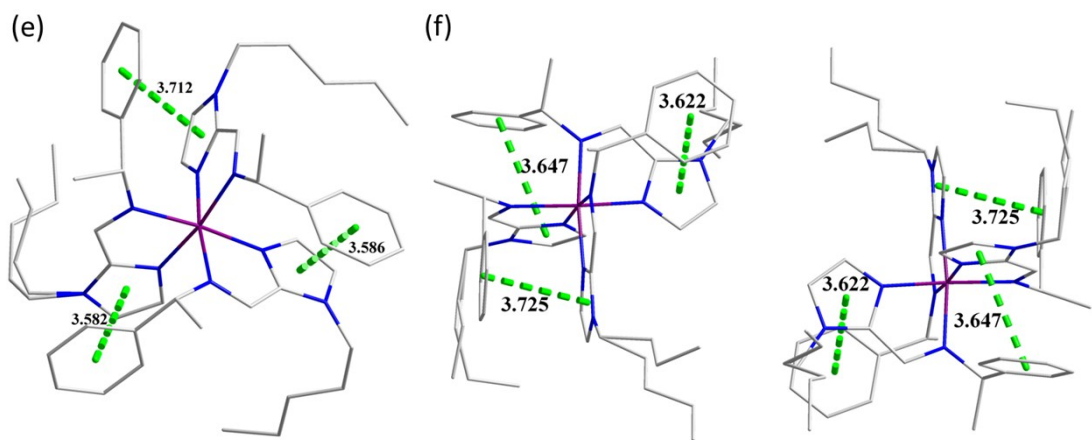


Fig. S2. Intramolecular π - π stacking interactions between imidazole and benzene rings in **4R** (a), **4RS** (b), **5R** (c), **5RS** (d), **4R5R** (e), and **4RS5RS** (f). Color code: C, gray; N, blue; Fe, violet; π - π stacking interaction, green dashed lines. Centriod-centriod distances of π - π interactions: **4R**: 4.089 Å; **4RS**: 3.632 Å, 3.686 Å, 3.720 Å; **5R**: 3.948 Å; **5RS**: 3.574 Å, 3.636 Å, 3.728 Å; **4R5R**: 3.582 Å, 3.586 Å, 3.712 Å; **4RS5RS**: 3.622 Å, 3.647 Å, 3.725 Å.

3. Intermolecular interactions

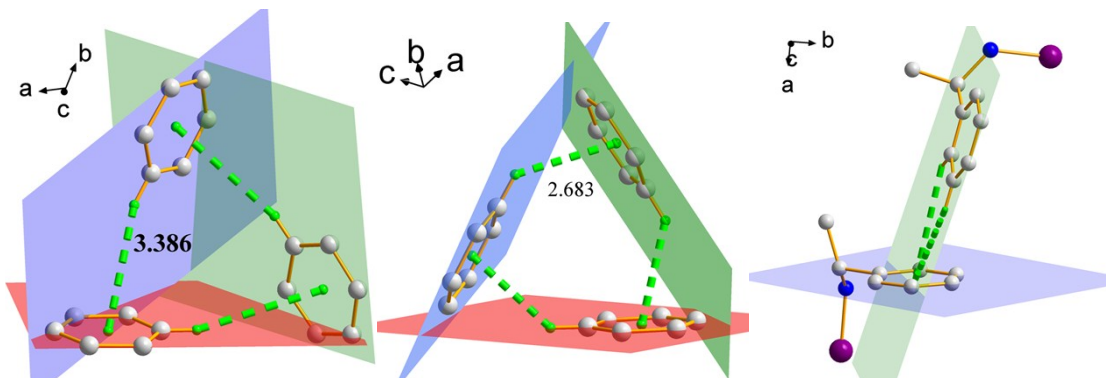


Fig. S3. Intermolecular C-H $\cdots\pi$ interaction mode in **4R** (left), **5R** (middle) and alloy complexes (right)

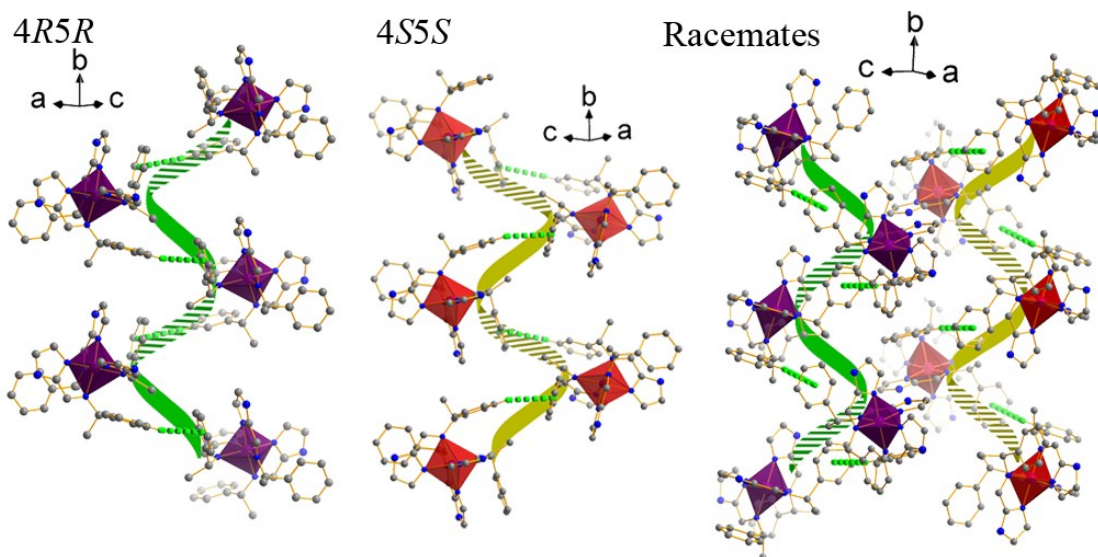


Fig. S4. Helical intermolecular interaction in molecular alloys/cocrystals.

In **4R5R**, one-dimensional left-handed helical chains are C-H $\cdots\pi$ bonded through the intermolecular interaction along *b* axis. On the contrary, metal cations of **4S5S** stack in right-handed helical one-dimensional chains via sequential intermolecular interaction. In crystals of **4RS**, **5RS** and **4RS5RS**, both left-handed and right-handed helical intermolecular interactions are discovered. In **R** layers, metal cations are arranged via one-dimensional left-handed helical C-H $\cdots\pi$ interactions while the **S** layers are linked by right-handed helical C-H $\cdots\pi$ interactions.

4. UV/Vis and CD spectra

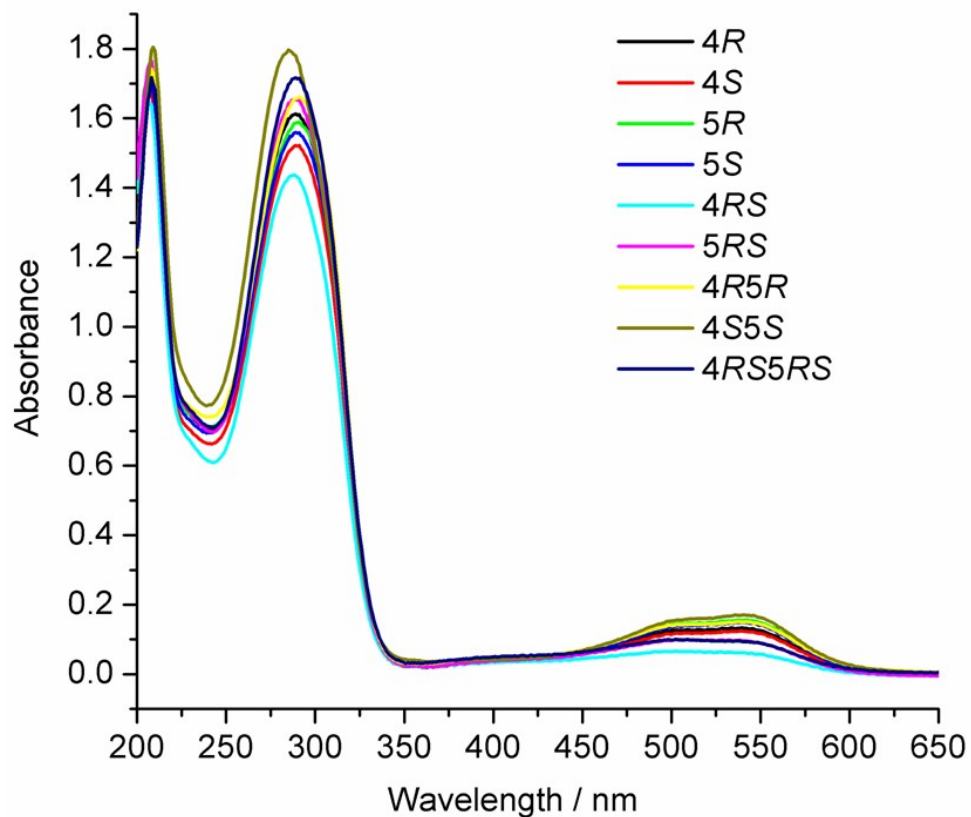


Fig. S5. UV/Vis spectra (10^{-5} M).

The UV/Vis spectra of the complexes are characterized by two $\pi-\pi^*$ transitions of imidazole and phenyl at 206-209 nm and 285-291 nm. Additionally, broad bands from 500 to 540 nm probably arise from the metal-to-ligand charge transfer (MLCT) process, which are indicative of the successful coordination and their low spin states in solution at room temperature.

Spin crossover in solution

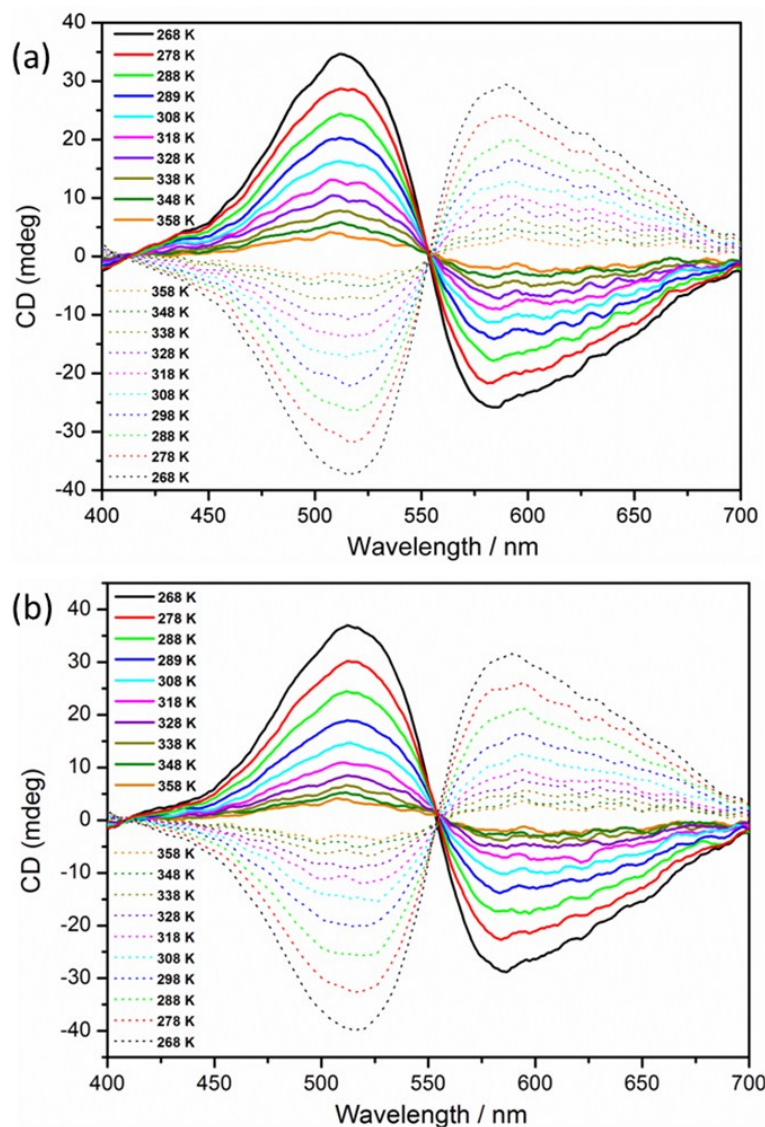
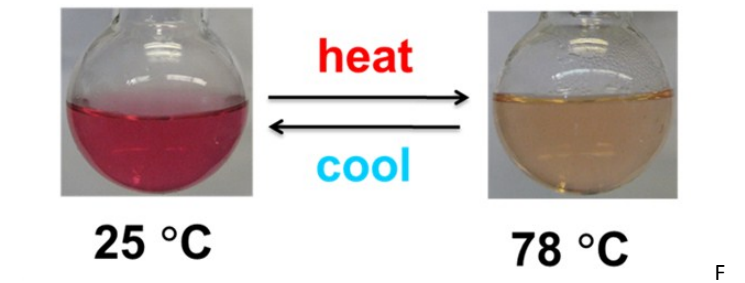


Fig. S6. Spin crossover in acetonitrile for **4R** and **4S** (10^{-4} M). Variable-temperature CD spectra of **4R** (solid) and **4S** (dash) in heating mode (a) and cooling mode (b). As temperature varied from 268 K to 358 K, the color of solution changes from red to light yellow while the MLCT sign varies from strong to weak. These phenomena suggest that the complexes exhibit SCO from LS state to HS state following the increasing temperature.

5. Thermogravimetric analyses (TGA)

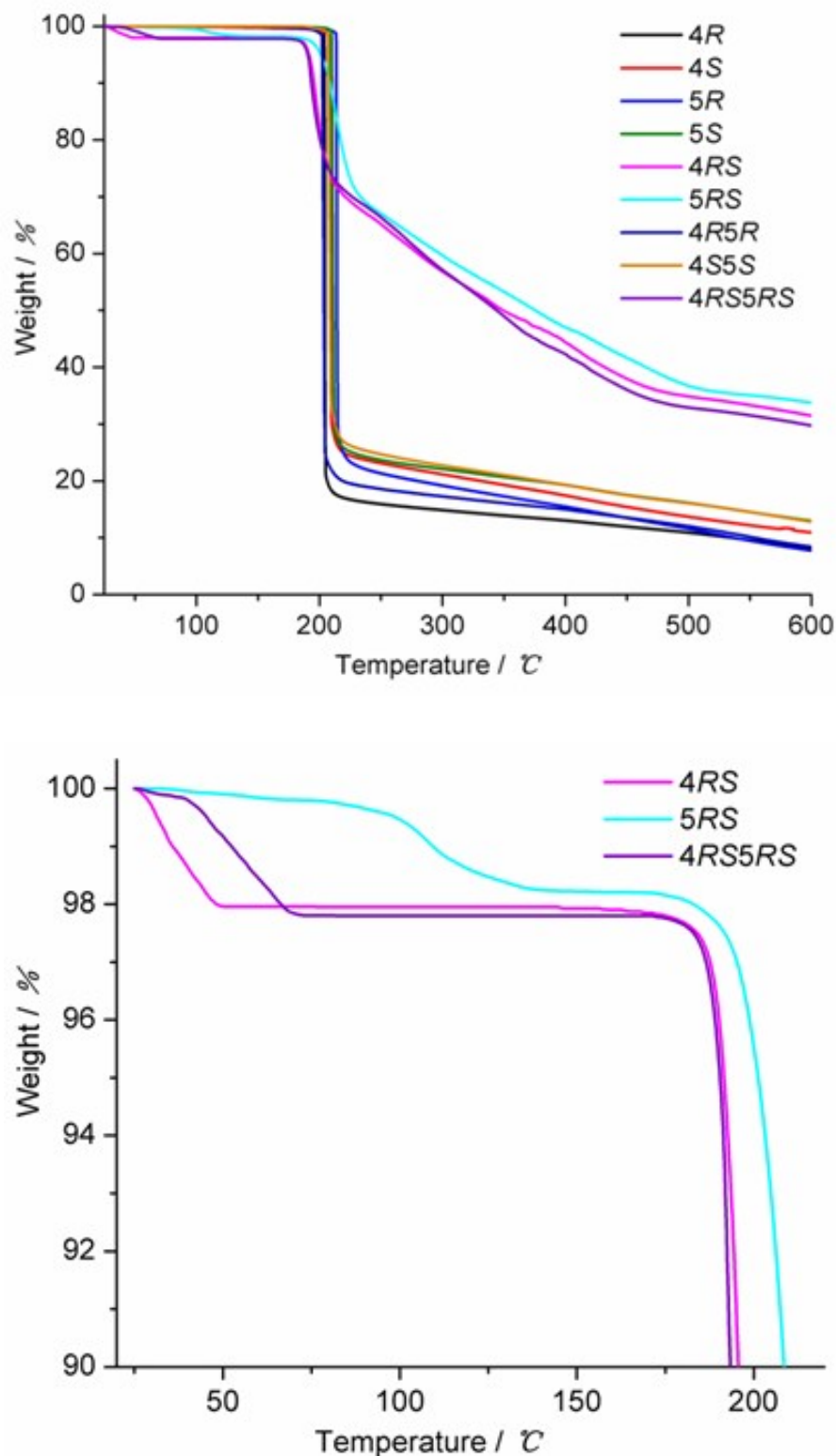


Fig. S7. TG analyses on all complexes (up) and the enlarged view in range of 25-200 °C for **4RS**, **5RS** and **4RS5RS** (down).

For solvent-free samples of **4R**, **4S**, **5R**, **5S**, **4R5R** and **4S5S**, their weights were nearly constant following the increasing temperature until 200 °C where the complexes started to decompose with abrupt losses of almost 75 percent of weight (**4R**: 83, **4S**: 75, **5R**: 76, **5S**: 74, **4R5R**: 80, **4S5S**: 73) in narrow temperature region of 200-220 °C. When heated to 600 °C, there were approximate 7-13 percent of weight residual, which possibly corresponded to the iron oxides.

According to the crystal structure analyses of **4RS**, **5RS** and **4RS5RS**, several solvent molecules were situated in their crystal lattices. For **4RS**, 0.17 acetonitrile and 0.83 diehtyl ether accounted for 6.27 percent of weight theoretically, however only 2.00 percent of weight was lost as the sample heating. This deviation was primarily caused by the rapid loss of diether ether at room temperature. Heating the sample of **5RS** resulted in a 1.80 percent of weight loss before 150 °C nearly to the calculated loss of 1.67 percent contributed by loss of one water molecule in the crystals. Sample of **4RS5RS** underwent a 2.20 percent of weight loss before 80 °C, with 0.77 acetonitrile accounting for 2.97 percent of weight theoretically. As samples were heated to the region of 200 °C to 600 °C, similar weight loss were observed for **4RS**, **5RS** and **4RS5RS**. About 26 percent of weight for **4RS** and **4RS5RS**, 30 percent for **5RS** lost rapidly around 230 °C, followed by further gradual weight loss until 500 °C. There were 31, 34 and 30 percent of the weight as residuals at 600 °C for **4RS**, **5RS** and **4RS5RS**, respectively.

6. Variable-temperature X-ray power diffraction profiles

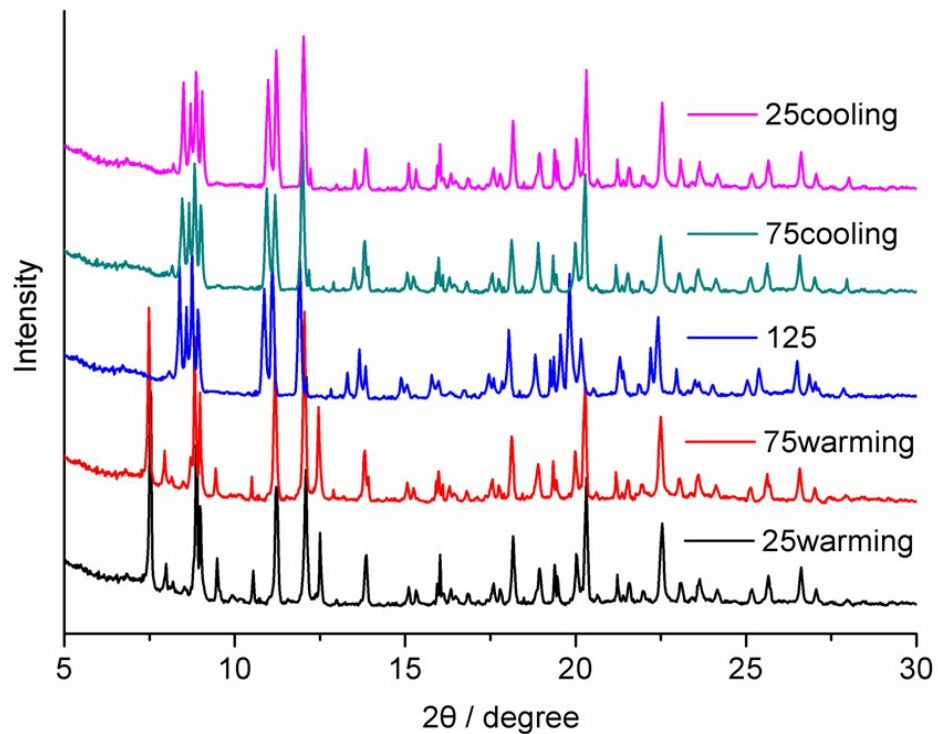


Fig. S8. Variable-temperature PXRD patterns of **5RS**.

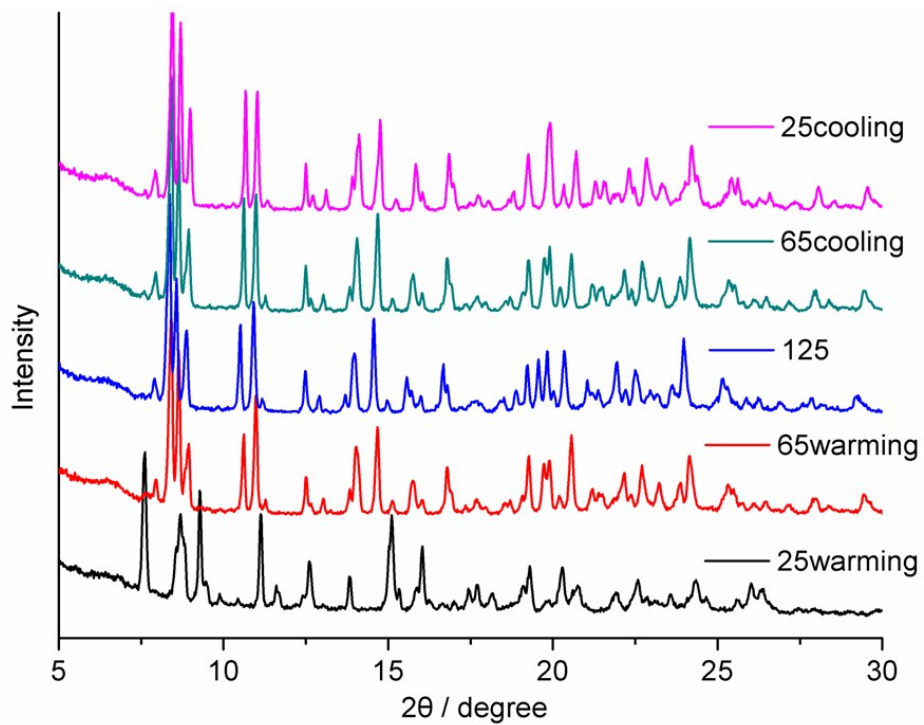


Fig. S9. Variable-temperature PXRD patterns of **4RS5RS**.

The variable-temperature PXRD patterns are collected in warming-cooling cycle. PXRD patterns of **5RS** are collected at 25 °C, 75 °C and 125 °C, while the PXRD pattern of **4RS5RS** is collected at 25 °C, 65 °C and 125 °C. The overall patterns are moving to the low angle as warmed towards high temperature, while moving to the high angle as cooled to low temperature. The crystallinity of **5RS** and **4RS5RS** are well maintained the in heating and warming suggesting their high stability for desolvated samples. For **5RS**, removal of uncoordinated water leads to a rearrangement of crystal lattices between 75 °C and 125 °C, involving the emergence of diffuse diffraction peaks at ca. 8.3 and 11.1° and the disappearance of peaks at ca.7.5, 7.8, 9.2 and 10.5°. For **4RS5RS**, the obvious change of profile between 25 °C and 65 °C is contributed by the loss the acetonitrile molecules. The new diffraction peaks mainly occur at ca. 8.1, 8.6, and 11.0°, while diffraction peaks at 7.5, 9.8, and 11.6° vanish as warming to 65 °C. The relative intensities of the Bragg diffraction maxima vary slightly in the warming-cooling mode, indicating the crystals do not undergo a collapse but a rearrangement. After the complete removal of solvent molecules, the overall PXRD patterns for **5RS** and **4RS5RS** simply exhibit a small shift in the following cooling mode.

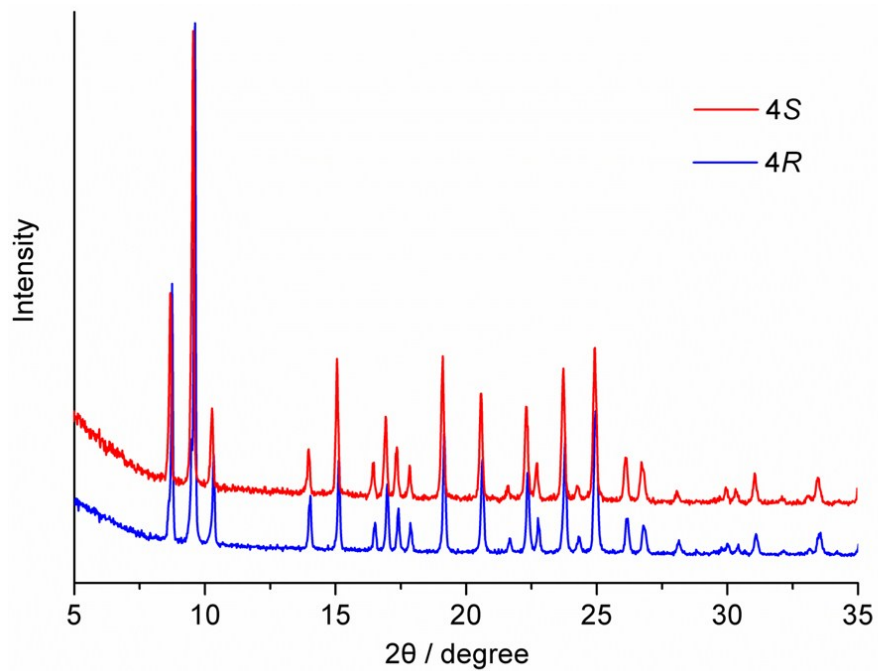


Fig. S10. PXRD patterns of **4R** (blue) and **4S** (red). All of the diffraction peaks are located in the same position for **4R** and **4S**.

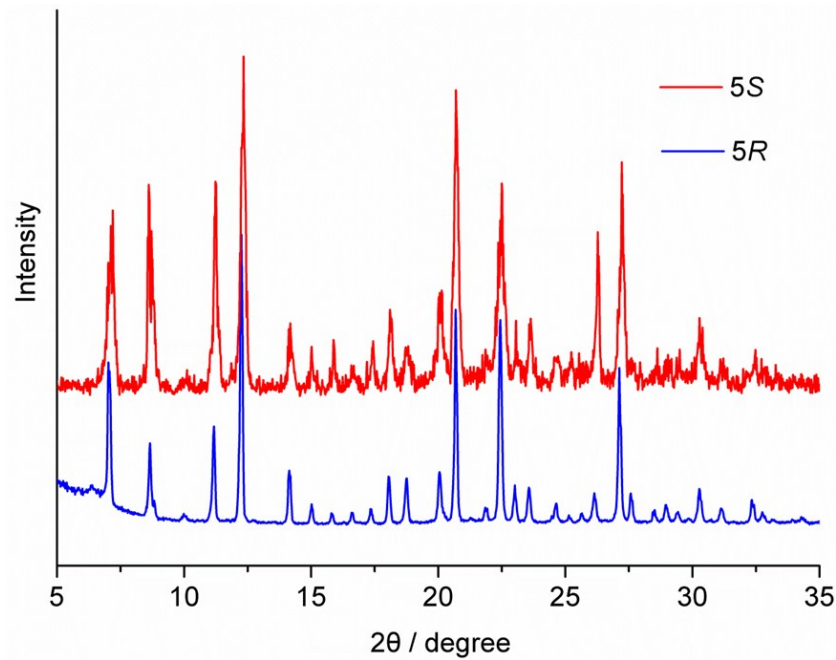


Fig. S11. PXRD patterns of **5R** (blue) and **5S** (red). All of the diffraction peaks are located in the same position for **5R** and **5S**.

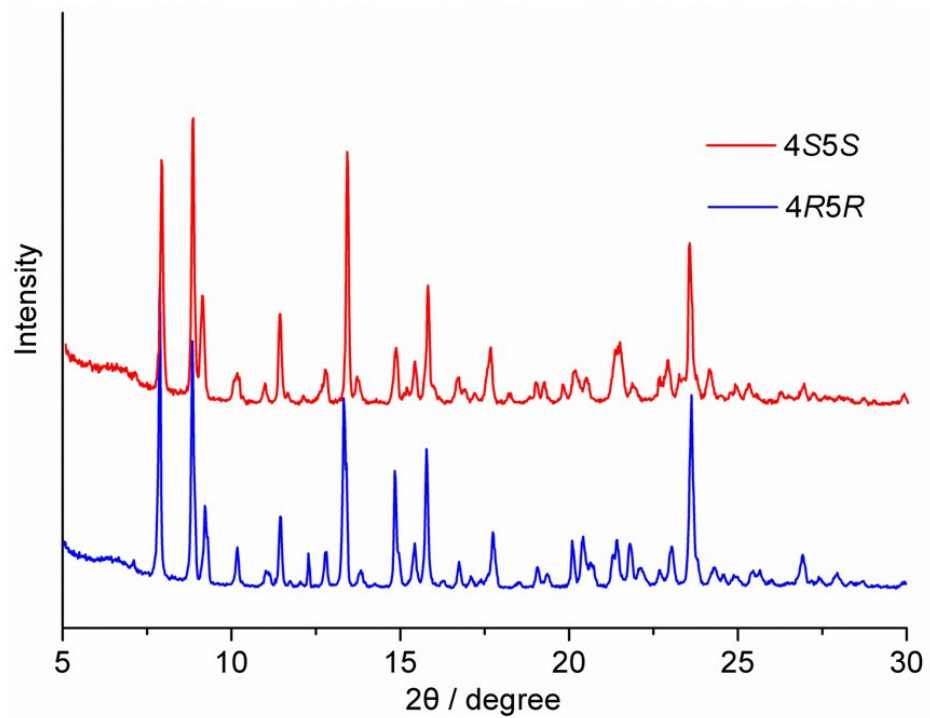


Fig. S12. PXRD patterns of **4R5R** (blue) and **4S5S** (red). All of the diffraction peaks are located in the same position for **4R5R** and **4S5S**.

7. Mössbauer data

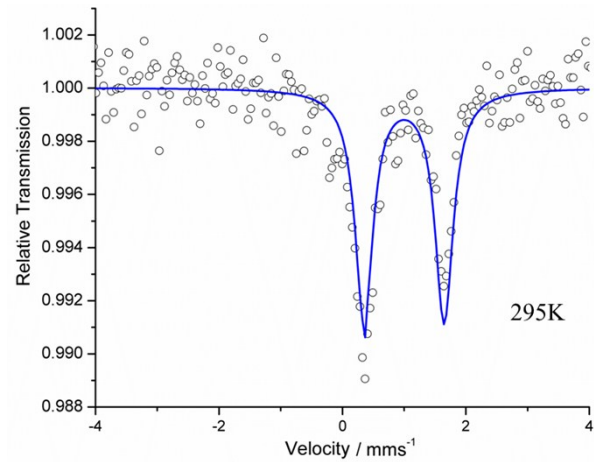


Fig. S13. Mössbauer spectrum of **4R** at 295K.

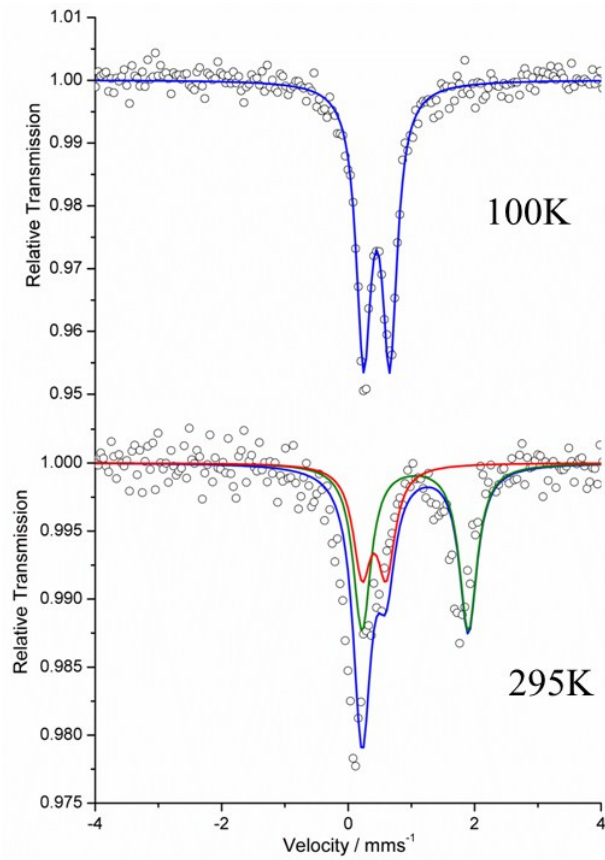


Fig. S14. Mössbauer spectra of **5R** at 100K and 295K.

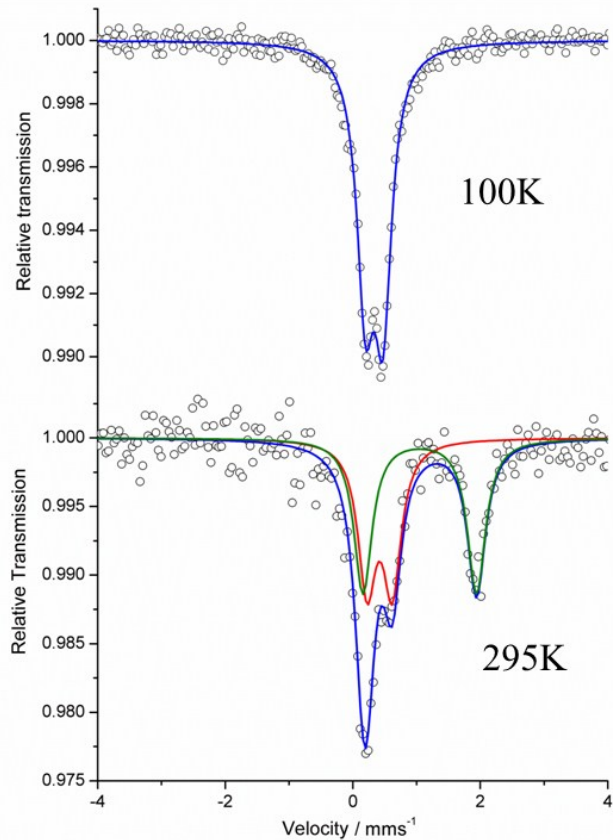


Fig. S15. Mössbauer spectra of **4R5R** at 100K and 295K.

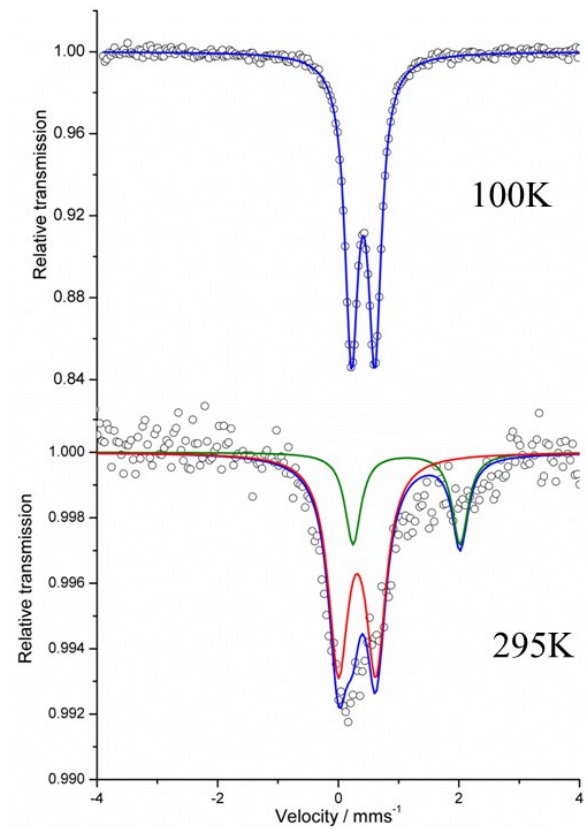


Fig. S16. Mössbauer spectra of **4RS** at 100K and 295K.

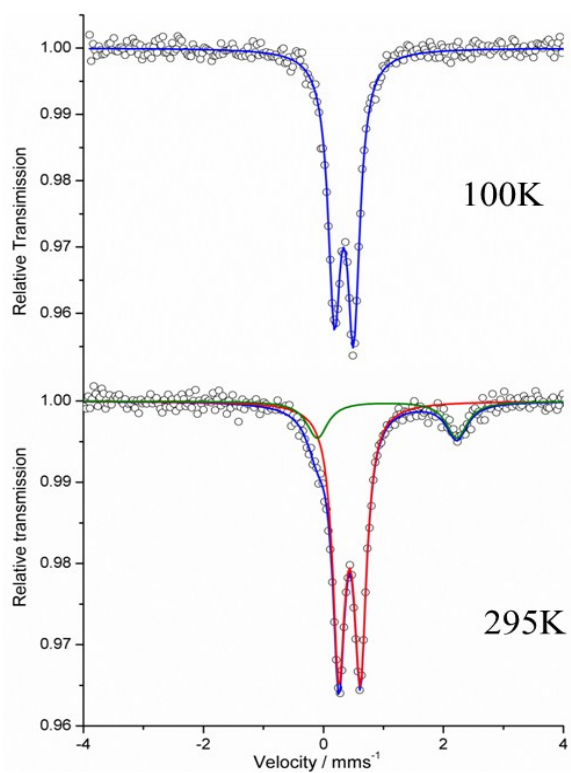


Fig. S17. Mössbauer spectra of **5RS** at 100K and 295K.

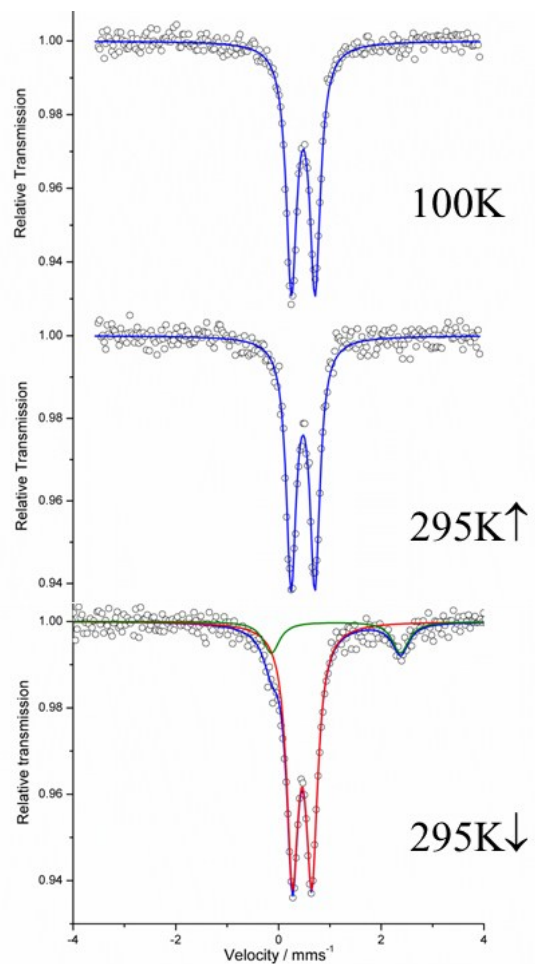


Fig. S18. Mössbauer spectra of **4RS5RS** at 100K and 295K.

Table S1. Summary of Mössbauer data for **4R**, **5R**, **4R5R**, **4RS**, **5RS** and **4RS5RS**

| $T(K)$ | $\delta(\text{mm}\cdot\text{s}^{-1})$ | $\Delta E_Q(\text{mm}\cdot\text{s}^{-1})$ | $I(\text{mm}\cdot\text{s}^{-1})$ | $A_{\text{HS}}/A_{\text{tot}}(\%)$ |
|---|---------------------------------------|---|----------------------------------|------------------------------------|
| 4R-295K | 1.00 | 1.30 | 0.35 | 100 |
| 5R-100K | 0.45 | 0.41 | 0.29 | 0 |
| 5R-295K | 1.06 0.41 | 1.68 0.38 | 0.34 0.41 | 57.78 |
| 4R5R-100K | 0.34 | 0.28 | 0.33 | 0 |
| 4R5R-295K | 1.05 0.42 | 1.78 0.40 | 0.35 0.34 | 46.90 |
| 4RS-100K | 0.41 | 0.39 | 0.26 | 0 |
| 4RS-295K | 1.13 0.31 | 1.77 0.62 | 0.31 0.40 | 24.26 |
| 5RS-100K | 0.34 | 0.32 | 0.25 | 0 |
| 5RS-295K | 1.05 0.44 | 2.31 0.36 | 0.40 0.26 | 20.32 |
| 4RS5RS-100K | 0.48 | 0.46 | 0.25 | 0 |
| 4RS5RS-295K\uparrow | 0.48 | 0.46 | 0.24 | 0 |
| 4RS5RS-295K\downarrow | 1.12 0.46 | 2.52 0.38 | 0.39 0.27 | 15.48 |

8. Crystallographic data

The crystal structures were determined on a Siemens (Bruker) SMART CCD diffractometer using monochromated Mo $K\alpha$ radiation ($\lambda = 0.71073 \text{ \AA}$) at 173 K or 296 K. Cell parameters were retrieved using SMART software and refined using SAINT^[1] on all observed reflections. The highly redundant data sets were reduced using SAINT and corrected for Lorentz and polarization effects. Absorption corrections were applied using SADABS^[2] supplied by Bruker. Structures were solved by direct methods using the program SHELXL-97^[3]. All of the non-hydrogen atoms except the anions, disordered solvent molecules and alkyl chains were refined with anisotropic thermal displacement coefficients. Hydrogen atoms of organic ligands were located geometrically and refined in a riding model, whereas those of solvent molecules were not treated during the structural refinements. Disorder was modeled using standard crystallographic methods including constraints, restraints and rigid bodies where necessary. For **4R** and **4S**, one of two perchlorate anions is disordered. Two perchlorate anions and two alkyl chains are disordered in **4RS**. Two perchlorate anion and one alkyl chains are disordered in **5RS**. Besides one disordered perchlorate anion in **4R5R**, the position of N-substituted alkyl chain is occupied by butyl and pentyl with almost equal probability in topology (butyl : pentyl = 54.6 : 45.4). Similarly, butyl and pentyl share the position of N-substituted alkyl chain in **4S5S** at a ratio of 45.8 : 54.2. While the probability distribution of N-substituted alkyl chain in **4S5R** is butyl : pentyl = 54.97 : 45.03, the probability of butyl and pentyl for **4R5S** in topology are 48.6 and 51.4 percent respectively.

Table S2. Summary of crystallographic data for **4R**, **4S**, **5R**, **5S** and **4RS**

| | 4R | 4S | 5R | 5S | 4RS |
|--|--|--|--|--|---|
| formula | C ₄₈ H ₆₃ Cl ₂ FeN ₉ O | C ₄₈ H ₆₃ Cl ₂ FeN ₉ O | C ₅₁ H ₆₉ Cl ₂ FeN ₉ O | C ₅₁ H ₆₉ Cl ₂ FeN ₉ O | C _{51.66} H _{71.80} Cl ₂ F |
| | 8 | 8 | 8 | 8 | eN _{9.17} O _{8.83} |
| fw | 1020.82 | 1020.82 | 1062.90 | 1062.90 | 1089.29 |
| crystal system | Trigonal | Trigonal | Cubic | Cubic | Monoclinic |
| space group | R ₃ | R ₃ | P2 ₁ 3 | P2 ₁ 3 | P2 ₁ /c |
| a (Å) | 12.7151(18) | 12.7337(12) | 17.4496(4) | 17.467(2) | 21.3124(16) |
| b (Å) | 12.7151(18) | 12.7337(12) | 17.4496(4) | 17.467(2) | 11.3534(7) |
| c (Å) | 28.077(4) | 28.004(2) | 17.4496(4) | 17.467(2) | 22.9705(18) |
| α (deg) | 90 | 90 | 90 | 90 | 90 |
| β (deg) | 90 | 90 | 90 | 90 | 99.571(2) |
| γ (deg) | 120 | 120 | 90 | 90 | 90 |
| Z | 3 | 3 | 4 | 4 | 4 |
| V (Å ³) | 3931.2(10) | 3932.4(6) | 5313.2(2) | 5328.9(11) | 5480.76(68) |
| D _{calcd} (g.cm ⁻³) | 1.294 | 1.293 | 1.329 | 1.325 | 1.32 |
| T (K) | 296(2) | 296(2) | 173(2) | 173(2) | 173(2) |
| μ (mm ⁻¹) | 0.448 | 0.448 | 0.445 | 0.444 | 0.434 |
| F(000) | 1614 | 1614 | 2248 | 2248 | 2306 |
| θ (deg) | 1.99-24.98 -15 ≤ h ≤ 7 | 1.98-24.99 -15 ≤ h ≤ 10 | 3.30-25.35 -16 ≤ h ≤ 20 | 3.30-24.95 -11 ≤ h ≤ 15 | 3.01-25.36 -25 ≤ h ≤ 25 |
| index ranges | -12 ≤ k ≤ 14 -33 ≤ l ≤ 27 | -10 ≤ k ≤ 15 -32 ≤ l ≤ 33 | -16 ≤ k ≤ 21 -20 ≤ l ≤ 20 | -12 ≤ k ≤ 20 -20 ≤ l ≤ 15 | -13 ≤ k ≤ 13 -27 ≤ l ≤ 23 |
| data/restraints /params | 2082 / 62 / 211 | 2994 / 1 / 207 | 3256 / 0 / 215 | 2735 / 0 / 216 | 9912 / 622 / 697 |
| GOF on F ² | 1.007 | 1.320 | 1.070 | 0.820 | 1.076 |
| R ₁ ^a [I > 2σ(I)] | 0.0501 | 0.0623 | 0.0534 | 0.0559 | 0.0792 |
| wR ₂ ^b [I > 2σ(I)] | 0.1381 | 0.1225 | 0.1377 | 0.1525 | 0.1999 |
| R ₁ ^a (all data) | 0.0527 | 0.0890 | 0.0868 | 0.0620 | 0.1584 |
| wR ₂ ^b (all data) | 0.1409 | 0.1467 | 0.1685 | 0.1633 | 0.2470 |
| Flack χ | 0.04(3) | -0.08(4) | -0.04(4) | -0.03(4) | |
| $R_1^a = \sum F_o - F_c / \sum F_o $. $wR_2^b = [\sum w(F_o^2 - F_c^2)^2 / \sum w(F_o^2)]^{1/2}$ | | | | | |

Table S3. Summary of crystallographic data for **5RS**, **4R5R**, **4S5S**, **4S5R** and **4R5S**

| | 5RS | 4R5R | 4S5S | 4S5R | 4R5S |
|---|--|---|---|---|---|
| formula | C ₅₁ H ₇₁ Cl ₂ FeN 9O ₉ | C _{49.36} H _{65.73} Cl ₂ Fe N ₉ O ₈ | C _{49.62} H _{66.25} Cl ₂ Fe N ₉ O ₈ | C _{50.90} H _{68.03} Cl ₂ FeN 9.77O ₈ | C _{51.10} H _{68.43} Cl ₂ FeN 9.78O ₈ |
| | | | | | |
| fw | 1078.90 | 1039.97 | 1043.62 | 1071.58 | 1074.52 |
| crystal system | Monoclinic | Monoclinic | Monoclinic | Monoclinic | Monoclinic |
| space group | <i>P</i> 2 ₁ /c | <i>P</i> 2 ₁ | <i>P</i> 2 ₁ | <i>P</i> 2 ₁ /c | <i>P</i> 2 ₁ /c |
| <i>a</i> (Å) | 20.1676(9) | 13.3549(9) | 13.3184(7) | 20.9361(17) | 20.9379(11) |
| <i>b</i> (Å) | 11.4224(5) | 11.2578(7) | 11.2564(6) | 11.3411(8) | 11.3072(5) |
| <i>c</i> (Å) | 23.5837(12) | 17.3499(13) | 17.3597(9) | 23.3530(2) | 23.3512(11) |
| α (deg) | 90 | 90 | 90 | 90 | 90 |
| β (deg) | 99.917(2) | 97.499(3) | 97.5679(18) | 99.474(3) | 99.493(2) |
| γ (deg) | 90 | 90 | 90 | 90 | 90 |
| <i>Z</i> | 4 | 2 | 2 | 4 | 4 |
| <i>V</i> (Å ³) | 5351.6(4) | 2586.2(3) | 2579.8(2) | 5469.3(8) | 5452.7(5) |
| <i>D</i> _{calcd} (g.cm ⁻³) | 1.339 | 1.335 | 1.343 | 1.301 | 1.309 |
| <i>T</i> (K) | 173(2) | 173(2) | 173(2) | 173(2) | 173(2) |
| μ (mm ⁻¹) | 0.444 | 0.456 | 0.457 | 0.433 | 0.435 |
| <i>F</i> (000) | 2280 | 1098 | 1102 | 2263 | 2270 |
| θ (deg) | 3.04-25.39 -24 ≤ <i>h</i> ≤ 24 | 2.98-25.39 -16 ≤ <i>h</i> ≤ 15 | 3.09-25.34 -15 ≤ <i>h</i> ≤ 16 | 3.19-24.25 -24 ≤ <i>h</i> ≤ 22 | 3.02-25.43 -25 ≤ <i>h</i> ≤ 25 |
| index ranges | -13 ≤ <i>k</i> ≤ 12 -28 ≤ <i>l</i> ≤ 28 | -11 ≤ <i>k</i> ≤ 13 -20 ≤ <i>l</i> ≤ 20 | -12 ≤ <i>k</i> ≤ 13 -20 ≤ <i>l</i> ≤ 20 | -13 ≤ <i>k</i> ≤ 13 -26 ≤ <i>l</i> ≤ 26 | -13 ≤ <i>k</i> ≤ 23 -26 ≤ <i>l</i> ≤ 28 |
| data/restraints/p | 9670 / 816 / 778 | 8155 / 336 / 725 | 8563 / 336 / 725 | 8649 / 989 / 843 | 9911 / 1137 / 866 |
| GOF on F ² | 1.146 | 1.160 | 1.026 | 1.090 | 1.292 |
| <i>R</i> ₁ ^a [<i>I</i> > 2σ(<i>I</i>)] | 0.0693 | 0.0769 | 0.0504 | 0.1050 | 0.0978 |
| w <i>R</i> ₂ ^b [<i>I</i> > 2σ(<i>I</i>)] | 0.1917 | 0.1400 | 0.0930 | 0.2283 | 0.2713 |
| <i>R</i> ₁ ^a (all data) | 0.1142 | 0.1259 | 0.0775 | 0.2112 | 0.1676 |
| w <i>R</i> ₂ ^b (all data) | 0.2292 | 0.1608 | 0.1038 | 0.2599 | 0.3246 |
| Flack <i>χ</i> | | -0.020(3) | -0.013(18) | | |
| <i>R</i> ₁ ^a = Σ <i>F</i> _o - <i>F</i> _c / Σ <i>F</i> _o . w <i>R</i> ₂ ^b = [Σw(<i>F</i> _o ² - <i>F</i> _c ²) ² / Σw(<i>F</i> _o ²)] ^{1/2} | | | | | |

Table S4. Selected bond lengths [Å] and angles [°] for **4R** and **4S**

| | 4R | | 4S |
|---------------------|------------|---------------------|------------|
| Fe(1)-N(2) | 2.133(4) | Fe(1)-N(1)#1 | 2.141(5) |
| Fe(1)-N(2)#3 | 2.133(4) | Fe(1)-N(1) | 2.141(5) |
| Fe(1)-N(2)#4 | 2.133(4) | Fe(1)-N(1)#2 | 2.141(5) |
| Fe(1)-N(3)#4 | 2.275(4) | Fe(1)-N(2)#2 | 2.271(5) |
| Fe(1)-N(3)#3 | 2.275(4) | Fe(1)-N(2) | 2.271(5) |
| Fe(1)-N(3) | 2.275(4) | Fe(1)-N(2)#1 | 2.271(5) |
| N(2)-Fe(1)-N(2)#3 | 91.49(18) | N(1)#1-Fe(1)-N(1) | 92.30(2) |
| N(2)-Fe(1)-N(2)#4 | 91.49(18) | N(1)#1-Fe(1)-N(1)#2 | 92.30(2) |
| N(2)#3-Fe(1)-N(2)#4 | 91.49(18) | N(1)-Fe(1)-N(1)#2 | 92.30(2) |
| N(2)-Fe(1)-N(3)#4 | 164.85(16) | N(1)#1-Fe(1)-N(2)#2 | 164.92(17) |
| N(2)#3-Fe(1)-N(3)#4 | 96.67(16) | N(1)-Fe(1)-N(2)#2 | 96.32(16) |
| N(2)#4-Fe(1)-N(3) | 75.61(15) | N(1)#2-Fe(1)-N(2)#2 | 75.08(16) |
| N(2)-Fe(1)-N(3)#3 | 96.67(16) | N(1)#1-Fe(1)-N(2) | 96.32(16) |
| N(2)#3-Fe(1)-N(3) | 75.61(15) | N(1)-Fe(1)-N(2) | 75.08(16) |
| N(2)#4-Fe(1)-N(3)#3 | 164.85(16) | N(1)#2-Fe(1)-N(2) | 164.92(17) |
| N(3)#4-Fe(1)-N(3)#3 | 97.70(14) | N(2)#2-Fe(1)-N(2) | 97.86(15) |
| N(2)-Fe(1)-N(3) | 75.61(15) | N(1)#1-Fe(1)-N(2)#1 | 75.08(16) |
| N(2)#3-Fe(1)-N(3) | 164.85(16) | N(1)-Fe(1)-N(2)#1 | 164.92(17) |
| N(2)#4-Fe(1)-N(3) | 96.67(16) | N(1)#2-Fe(1)-N(2)#1 | 96.32(16) |
| N(3)#4-Fe(1)-N(3) | 97.70(14) | N(2)#2-Fe(1)-N(2)#1 | 97.86(15) |
| N(3)#3-Fe(1)-N(3) | 97.70(14) | N(2)-Fe(1)-N(2)#1 | 97.86(15) |

Symmetry transformations used to generate equivalent atoms for **4R**: #3 -x+y, -x, z, #4 -y, x-y, z;
 for **4S**: #1 -y+2, x-y+1, z; #2 -x+y+1, -x+2, z.

Table S5. Selected bond lengths [Å] and angles [°] for **5R** and **5S**

| | 5R | | 5S |
|---------------------|------------|---------------------|------------|
| Fe(1)-N(1) | 1.944(4) | Fe(1)-N(1) | 1.960(4) |
| Fe(1)-N(1)#5 | 1.945(4) | Fe(1)-N(1)#1 | 1.960(4) |
| Fe(1)-N(1)#6 | 1.945(4) | Fe(1)-N(1)#2 | 1.960(4) |
| Fe(1)-N(3) | 2.030(4) | Fe(1)-N(3) | 2.046(4) |
| Fe(1)-N(3)#6 | 2.030(4) | Fe(1)-N(3)#2 | 2.046(4) |
| Fe(1)-N(3)#5 | 2.030(4) | Fe(1)-N(3)#1 | 2.046(4) |
| N(1)-Fe(1)-N(1)#5 | 89.90(17) | N(1)-Fe(1)-N(1)#1 | 90.41(19) |
| N(1)-Fe(1)-N(1)#6 | 89.90(17) | N(1)-Fe(1)-N(1)#2 | 90.41(18) |
| N(1)#5-Fe(1)-N(1)#6 | 89.90(17) | N(1)#1-Fe(1)-N(1)#2 | 90.41(18) |
| N(1)-Fe(1)-N(3) | 80.36(15) | N(1)-Fe(1)-N(3) | 79.98(17) |
| N(1)#5-Fe(1)-N(3) | 90.76(15) | N(1)#1-Fe(1)-N(3) | 170.24(18) |
| N(1)#6-Fe(1)-N(3) | 170.23(16) | N(1)#2-Fe(1)-N(3) | 91.35(17) |
| N(1)-Fe(1)-N(3)#6 | 90.76(15) | N(1)-Fe(1)-N(3)#2 | 170.24(18) |
| N(1)#5-Fe(1)-N(3)#6 | 170.23(16) | N(1)#1-Fe(1)-N(3)#2 | 91.35(16) |
| N(1)#6-Fe(1)-N(3)#6 | 80.35(15) | N(1)#2-Fe(1)-N(3)#2 | 79.98(17) |
| N(3)-Fe(1)-N(3)#6 | 98.96(14) | N(3)-Fe(1)-N(3)#2 | 98.40(16) |
| N(1)-Fe(1)-N(3)#5 | 170.23(16) | N(1)-Fe(1)-N(3)#1 | 91.35(17) |
| N(1)#5-Fe(1)-N(3)#5 | 80.35(15) | N(1)#1-Fe(1)-N(3)#1 | 79.98(17) |
| N(1)#6-Fe(1)-N(3)#5 | 90.76(15) | N(1)#2-Fe(1)-N(3)#1 | 170.24(18) |
| N(3)-Fe(1)-N(3)#5 | 98.96(14) | N(3)-Fe(1)-N(3)#1 | 98.40(16) |
| N(3)#6-Fe(1)-N(3)#5 | 98.96(14) | N(3)#2-Fe(1)-N(3)#1 | 98.40(16) |

Symmetry transformations used to generate equivalent atoms for **5R**: #5 -z+3/2, -x+1, y+1/2; #6 -y+1, z-1/2, -x+3/2; for **5S**: #1 -z, x+1/2, -y+1/2; #2 y-1/2, -z+1/2, -x.

Table S6. Selected bond lengths [Å] and angles [°] for **4RS** and **5RS**

| | 4RS | | 5RS |
|-----------------|------------|-----------------|------------|
| Fe(2)-N(7) | 1.946(5) | Fe(1)-N(1) | 1.948(4) |
| Fe(2)-N(1) | 1.951(5) | Fe(1)-N(4) | 1.953(4) |
| Fe(2)-N(4) | 1.960(5) | Fe(1)-N(7) | 1.959(4) |
| Fe(2)-N(6) | 1.980(5) | Fe(1)-N(6) | 1.987(4) |
| Fe(2)-N(3) | 2.005(4) | Fe(1)-N(9) | 2.001(4) |
| Fe(2)-N(9) | 2.007(5) | Fe(1)-N(3) | 2.010(3) |
| N(7)-Fe(2)-N(1) | 91.40(2) | N(1)-Fe(1)-N(4) | 91.65(15) |
| N(7)-Fe(2)-N(4) | 92.50(2) | N(1)-Fe(1)-N(7) | 91.21(16) |
| N(1)-Fe(2)-N(4) | 91.68(19) | N(4)-Fe(1)-N(7) | 91.50(15) |
| N(7)-Fe(2)-N(6) | 172.55(19) | N(1)-Fe(1)-N(6) | 92.73(14) |
| N(1)-Fe(2)-N(6) | 92.63(19) | N(4)-Fe(1)-N(6) | 81.12(15) |
| N(4)-Fe(2)-N(6) | 81.12(19) | N(7)-Fe(1)-N(6) | 171.72(15) |
| N(7)-Fe(2)-N(3) | 92.47(18) | N(1)-Fe(1)-N(9) | 171.30(15) |
| N(1)-Fe(2)-N(3) | 80.72(18) | N(4)-Fe(1)-N(9) | 91.87(15) |
| N(4)-Fe(2)-N(3) | 171.03(19) | N(7)-Fe(1)-N(9) | 80.74(16) |
| N(6)-Fe(2)-N(3) | 94.38(17) | N(6)-Fe(1)-N(9) | 95.67(14) |
| N(7)-Fe(2)-N(9) | 80.80(2) | N(1)-Fe(1)-N(3) | 80.63(14) |
| N(1)-Fe(2)-N(9) | 171.63(19) | N(4)-Fe(1)-N(3) | 170.87(15) |
| N(4)-Fe(2)-N(9) | 91.67(18) | N(7)-Fe(1)-N(3) | 93.50(14) |
| N(6)-Fe(2)-N(9) | 95.46(18) | N(6)-Fe(1)-N(3) | 94.31(14) |
| N(3)-Fe(2)-N(9) | 96.51(18) | N(9)-Fe(1)-N(3) | 96.46(14) |

Table S7. Selected bond lengths [Å] and angles [°] for **4R5R** and **4S5S**

| | 4R5R | | 4S5S |
|-------------------|-------------|-------------------|-------------|
| Fe(1)-N(1A) | 1.933(6) | Fe(1)-N(1B) | 1.949(3) |
| Fe(1)-N(1C) | 1.964(6) | Fe(1)-N(1A) | 1.956(4) |
| Fe(1)-N(1B) | 1.965(5) | Fe(1)-N(1C) | 1.957(3) |
| Fe(1)-N(3B) | 1.979(6) | Fe(1)-N(3A) | 1.984(4) |
| Fe(1)-N(3A) | 1.993(7) | Fe(1)-N(3B) | 1.987(3) |
| Fe(1)-N(3C) | 2.001(5) | Fe(1)-N(3C) | 1.993(3) |
| N(1A)-Fe(1)-N(1C) | 91.40(3) | N(1B)-Fe(1)-N(1A) | 91.68(14) |
| N(1A)-Fe(1)-N(1B) | 91.60(2) | N(1B)-Fe(1)-N(1C) | 94.11(14) |
| N(1C)-Fe(1)-N(1B) | 94.40(2) | N(1A)-Fe(1)-N(1C) | 91.57(15) |
| N(1A)-Fe(1)-N(3B) | 172.40(2) | N(1B)-Fe(1)-N(3A) | 90.68(13) |
| N(1C)-Fe(1)-N(3B) | 91.10(2) | N(1A)-Fe(1)-N(3A) | 81.38(15) |
| N(1B)-Fe(1)-N(3B) | 81.10(2) | N(1C)-Fe(1)-N(3A) | 171.60(15) |
| N(1A)-Fe(1)-N(3A) | 81.20(3) | N(1B)-Fe(1)-N(3B) | 81.34(14) |
| N(1C)-Fe(1)-N(3A) | 171.00(3) | N(1A)-Fe(1)-N(3B) | 172.69(13) |
| N(1B)-Fe(1)-N(3A) | 90.80(2) | N(1C)-Fe(1)-N(3B) | 91.09(14) |
| N(3B)-Fe(1)-N(3A) | 96.90(2) | N(3A)-Fe(1)-N(3B) | 96.46(14) |
| N(1A)-Fe(1)-N(3C) | 92.10(2) | N(1B)-Fe(1)-N(3C) | 174.13(14) |
| N(1C)-Fe(1)-N(3C) | 81.30(2) | N(1A)-Fe(1)-N(3C) | 92.28(13) |
| N(1B)-Fe(1)-N(3C) | 174.40(3) | N(1C)-Fe(1)-N(3C) | 81.46(14) |
| N(3B)-Fe(1)-N(3C) | 95.40(2) | N(3A)-Fe(1)-N(3C) | 94.20(14) |
| N(3A)-Fe(1)-N(3C) | 93.9(2) | N(3B)-Fe(1)-N(3C) | 94.84(13) |

Table S8. Selected bond lengths [Å] and angles [°] for **4S5R** and **4R5S**

| | 4S5R | | 4R5S |
|-------------------|-------------|-------------------|-------------|
| Fe(1)-N(1A) | 1.940(6) | Fe(1)-N(1A) | 1.945(5) |
| Fe(1)-N(1C) | 1.940(6) | Fe(1)-N(1C) | 1.945(5) |
| Fe(1)-N(1B) | 1.959(6) | Fe(1)-N(1B) | 1.949(5) |
| Fe(1)-N(3B) | 1.970(6) | Fe(1)-N(3A) | 1.979(5) |
| Fe(1)-N(3C) | 1.993(6) | Fe(1)-N(3B) | 1.989(5) |
| Fe(1)-N(3A) | 1.995(6) | Fe(1)-N(3C) | 2.002(5) |
| N(1A)-Fe(1)-N(1C) | 91.20(3) | N(1A)-Fe(1)-N(1C) | 92.0(2) |
| N(1A)-Fe(1)-N(1B) | 92.30(3) | N(1A)-Fe(1)-N(1B) | 91.1(2) |
| N(1C)-Fe(1)-N(1B) | 91.20(3) | N(1C)-Fe(1)-N(1B) | 91.50(2) |
| N(1A)-Fe(1)-N(3B) | 172.80(3) | N(1A)-Fe(1)-N(3A) | 81.20(2) |
| N(1C)-Fe(1)-N(3B) | 92.40(2) | N(1C)-Fe(1)-N(3A) | 172.40(2) |
| N(1B)-Fe(1)-N(3B) | 81.40(3) | N(1B)-Fe(1)-N(3A) | 92.00(2) |
| N(1A)-Fe(1)-N(3C) | 92.50(2) | N(1A)-Fe(1)-N(3B) | 170.80(2) |
| N(1C)-Fe(1)-N(3C) | 81.30(2) | N(1C)-Fe(1)-N(3B) | 92.70(2) |
| N(1B)-Fe(1)-N(3C) | 171.30(3) | N(1B)-Fe(1)-N(3B) | 80.90(2) |
| N(3B)-Fe(1)-N(3C) | 94.20(2) | N(3A)-Fe(1)-N(3B) | 94.47(19) |
| N(1A)-Fe(1)-N(3A) | 81.30(3) | N(1A)-Fe(1)-N(3C) | 91.60(2) |
| N(1C)-Fe(1)-N(3A) | 172.00(3) | N(1C)-Fe(1)-N(3C) | 81.10(2) |
| N(1B)-Fe(1)-N(3A) | 91.80(3) | N(1B)-Fe(1)-N(3C) | 172.20(2) |
| N(3B)-Fe(1)-N(3A) | 95.30(2) | N(3A)-Fe(1)-N(3C) | 95.59(19) |
| N(3C)-Fe(1)-N(3A) | 96.10(2) | N(3B)-Fe(1)-N(3C) | 96.89(19) |

9. References

- [1] *SAINT-Plus*, version 6.02; Bruker Analytical X-ray System: Madison, WI, **1999**.
- [2] G. M. Sheldrick, *SADABS An empirical absorption correction program*; Bruker Analytical X-ray Systems: Madison, WI, **1996**.
- [3] G. M. Sheldrick, *SHELXTL-97*; Universität of Göttingen: Göttingen, Germany, **1997**.